Sensitivity of the NMR density matrix to pulse sequence parameters: A simplified analytic approach

Konstantin I. Momot*[1] and K. Takegoshi[2]

[1] School of Chemistry, Physics and Mechanical Engineering,
Queensland University of Technology,
GPO Box 2434, Brisbane, Qld 4001, Australia;

[2] Department of Chemistry, Graduate School of Science, Kyoto University, Kyoto, Japan

*Address for correspondence:	Konstantin I. Momot
	School of Chemistry, Physics and Mechanical Engineering
	Queensland University of Technology
	GPO Box 2434
	Brisbane, Qld 4001
	Australia,
E-mail address:	k.momot@qut.edu.au
Fax:	+61 7 3138 1521

Running title: Robustness of NMR Pulse Sequences

Revised version 25/04/2012 11:31 AM

Keywords: Nuclear Magnetic Resonance;
spin density matrix; product operator formalism;
unitary transformation;
NMR quantum computing;
NMR pulse sequence design

Key abbreviations and symbols:

CTP, coherence transfer pathway;
DM, density matrix;
DQ, double-quantum;
ECF, error commutator formalism;
H_i, Hamiltonian during interval i;
J, scalar coupling constant;
NMR, Nuclear Magnetic Resonance;
PO, product operator;
RF, radiofrequency;
SQ, single-quantum;
t_i, duration of interval i;
U_i, unitary evolution operator during interval i;
ZQ, zero-quantum;
$\theta_i = \omega_i t_i$, generalised time corresponding to interval i;
ρ_i, density matrix at the end of interval i;
ω_i, amplitude of interaction under the Hamiltonian H_i.

Abstract

We present a formalism for the analysis of sensitivity of nuclear magnetic resonance pulse sequences to variations of pulse sequence parameters, such as radiofrequency pulses, gradient pulses or evolution delays. The formalism enables the calculation of compact, analytic expressions for the derivatives of the density matrix and the observed signal with respect to the parameters varied. The analysis is based on two constructs computed in the course of modified density-matrix simulations: the *error interrogation operators* and *error commutators*. The approach presented is consequently named the Error Commutator Formalism (ECF). It is used to evaluate the sensitivity of the density matrix to parameter variation based on the simulations carried out for the *ideal* parameters, obviating the need for finite-difference calculations of signal errors. The ECF analysis therefore carries a computational cost comparable to a single density-matrix or product-operator simulation. Its application is illustrated using a number of examples from basic NMR spectroscopy. We show that the strength of the ECF is its ability to provide analytic insights into the propagation of errors through pulse sequences and the behaviour of signal errors under phase cycling. Furthermore, the approach is algorithmic and easily amenable to implementation in the form of a programming code. It is envisaged that it could be incorporated into standard NMR product-operator simulation packages.

INTRODUCTION

Recently Kuprov and Rodgers presented an analytic formalism for the evaluation of derivatives of NMR spin density matrix (DM) with respect to pulse sequence and spin system parameters [1]. They specifically identified two scenarios where the knowledge of DM derivatives is advantageous: (1) spectral fitting and (2) pulse sequence design using optimal control theory. The knowledge of DM derivatives also enables the analysis of sensitivity of NMR measurements to miscalibration of pulse sequence parameters, which is useful for the evaluation of robustness of quantitative NMR measurements of diffusion coefficients, spin relaxation rates and similar properties.

Kuprov and Rodgers' formalism is exact, in that the evolution of the spin system in it includes both reversible Hamiltonian dynamics and irreversible dynamics such as spin relaxation and chemical kinetics. Because of its exact nature, DM derivatives in that formalism can be difficult to obtain in closed analytic form. In this work, we present a simplified approach to the calculation of DM derivatives that neglects spin relaxation and kinetics. The simplified approach is named the Error Commutator Formalism (ECF), owing to the fact that the derivatives of the DM are computed as commutators of the appropriate operators with the spin density matrix. The ECF is amenable to non-numerical analysis and yields compact analytic expressions for DM derivatives. The approach is also intuitive in that it can be used to analyse the contributions to DM derivatives arising from different coherence transfer pathways. The relationship of the ECF to the exact formalism by Kuprov and Rodgers can be compared to the relationship between the simplified Product-Operator and the exact Density-Matrix treatments of NMR experiments. In this respect the ECF is complementary to Kuprov and Rodgers' formalism.

In this paper we use the ECF to explore the behaviour of errors of the DM and the observed signal in various experimental NMR scenarios. The "errors" are defined, in general, in the sense of the Taylor expansion truncated to the appropriate number of terms. The Theory section of the paper presents the basics of the ECF, including specific equations for the evaluation of DM derivatives with respect to RF pulse flip angles, resonance offsets and RF pulse phase errors. In Results and Discussion we illustrate application of the ECF using a number of examples from practical NMR spectroscopy. We show that the ECF can provide analytic insights into the propagation of errors through pulse sequences and the behaviour of errors under phase cycling.

THEORY

Consider a NMR experiment represented by a sequence of RF pulses, gradient pulses and delays (to which we shall collectively refer as "intervals"), as illustrated in Fig. 1. If the rotating-frame spin Hamiltonian during each interval is constant, then, following the standard NMR density matrix (DM) formalism [2], the evolution of the spin density matrix during the k-th interval can be represented by the unitary evolution operator:

$$U_k = e^{iH_k\theta_k} \tag{1}$$

Here, H_k is the dimensionless spin Hamiltonian containing only the appropriate spin operators. The amplitude of the respective interaction (ω_k) is incorporated in the parameter $\theta_k = \omega_k t_k$, which we refer to as the dimensionless *generalised time*. For example, if the interval k is an RF pulse, then $\theta_k = \gamma B_1 t_k$, where t_k is the physical duration of the pulse, and $H_k = I_x$ or I_y. The generalised times θ_k therefore have the meaning of rotation angles. The operator H_k need not be a "simple" spin operator and may itself contain non-commuting terms, such as the dipolar-coupling or the strong scalar-coupling Hamiltonians.

Neglecting spin relaxation and chemical kinetics, the effect of the entire pulse sequence on the spin density matrix can be represented as a unitary transformation

$$\rho_n = U^+\rho_0 U \tag{2}$$

where $\rho_0 = I_z$ is the initial DM; ρ_n is the DM at the end of the pulse sequence; and

$$U = e^{iH_1\theta_1}\cdot e^{iH_2\theta_2}\ldots e^{iH_n\theta_n} = \prod_{k=1}^{n} U_k \tag{3}$$

The central question considered in the present work is the following: What is the effect of a mis-set generalised time θ_k on the signal detected at the end of the pulse sequence? The first derivative of ρ_n with respect to θ_k can be generally written as:

$$\frac{\partial\rho_n}{\partial\theta_k} = e^{-iH_n\theta_n}\ldots(-iH_k)e^{-iH_k\theta_k}\ldots e^{-iH_1\theta_1}\rho_0 e^{iH_1\theta_1}\ldots e^{iH_n\theta_n} + e^{-iH_n\theta_n}\ldots e^{-iH_1\theta_1}\rho_0 e^{iH_1\theta_1}\ldots e^{iH_k\theta_k}(iH_k)\ldots e^{iH_n\theta_n} \tag{4}$$

In order to make Eq. (4) amenable to interpretation, we introduce the following identity operators:

$$\begin{aligned}\hat{1}_k &= U_k U_k^+ = e^{iH_k\theta_k}\cdot e^{-iH_k\theta_k}\\ \hat{1}_k^+ &= U_k^+ U_k = e^{-iH_k\theta_k}\cdot e^{iH_k\theta_k}\end{aligned} \tag{5}$$

Sequentially inserting the identity operators from 1_{k+1} to 1_n between U_k and H_k in Eq. (4):

$$\begin{gathered}U_n^+ ... U_1^+ \cdot \rho_0 \cdot U_1 ... U_k \cdot (iH_k) ... U_n\\ \wedge\\ e^{iH_{k+1}\theta_{k+1}}\cdot e^{-iH_{k+1}\theta_{k+1}}\\ \wedge\\ e^{iH_{k+2}\theta_{k+2}}\cdot e^{-iH_{k+2}\theta_{k+2}}\\ \wedge\\ \text{...etc. up to } \hat{1}_n\end{gathered} \tag{6}$$

we obtain:

$$\frac{\partial \rho_n}{\partial \theta_k} = i\cdot\left[\rho_n,\, U_n^+ ... U_{k+1}^+ \cdot H_k \cdot U_{k+1} ... U_n\right] \equiv i\cdot\left[\rho_n,\, H_k^*\left(k+1:n\right)\right] \tag{7}$$

where H_k*(k+1:n) is the unitary-transformed spin Hamiltonian H_k:

$$H_k^*\left(k+1:n\right) = U_n^+ ... U_{k+1}^+ \cdot H_k \cdot U_{k+1} ... U_n \tag{8}$$

In the following, we refer to the operator H_k^*(k+1:n) as the *error interrogation operator*: As is evident from Eq. (7), it determines whether $\partial\rho_n/\partial\theta_k$ is non-zero. The coherences contained in $\partial\rho_n/\partial\theta_k$ determine whether a non-zero derivative of the DM leads to a variation of the observable signal.

The error commutator formalism (ECF) encompassed by Eqs. (4) – (8) is similar to the formalism recently presented by Kuprov and Rodgers [1]. The difference between the two approaches is that ECF neglects the irreversible dynamics of spins (such as spin relaxation and chemical reactions). As will be seen below, the strength of the ECF lies in its ability to provide analytic insights into the propagation of errors arising from individual elements of the pulse sequence through the pulse sequence, as well as the behaviour of errors under phase cycling.

ECF is complementary to the approach by Kuprov and Rodgers, whose strength is in the exact numerical treatment of the errors, including the effects of relaxation and kinetics. In this respect ECF relates to the latter approach in the way similar to the relationship between the simplified product-operator formalism and the exact density-matrix formalism.

Similar to Eq. (6), the operators from 1^{+}_{k-1} to 1_{1}^{+} can be inserted on the inside of $e^{\pm iH_k\theta_k}$ in Eq. (4) . This enables the variation of ρ_n to be expressed via the initial DM:

$$\frac{\partial \rho_n}{\partial \theta_k} = i(U_n^+ ... U_1^+) \cdot [\rho_0, H_k^*(k-1:1)] \cdot (U_1 ... U_n) \tag{9}$$

where H_k*(k–1:1) is the reverse-transformed dimensionless Hamiltonian H_k:

$$H_k^*(k-1:1) = U_1 ... U_{k-1} \cdot H_k \cdot U_{k-1}^+ ... U_1^+ \tag{10}$$

Selection rules. The DM derivative given by Eq. (7) can contain both observable and non-observable terms. The relationship between the derivative of the final density matrix (ρ_n) and the derivative of the complex observed signal (S) is

$$\frac{\partial S}{\partial \theta_k} = Tr\left[I_-^+ \cdot \frac{\partial \rho_n}{\partial \theta_k} \right] \tag{11}$$

where $I_-^+ = I_+$ is the Hermitian conjugate of the observable operator I_-. The observable operator in Eq. (11) needs to be taken as the Hermitian conjugate because the complex operator I_- is used as the observable rather than the real operators I_x, I_y; this is readily apparent from the example of a single spin-1/2 and $\rho_n = I_-$: in this simple case, Tr[$I_-^+ \cdot I_-$] = 1 while Tr[$I_- \cdot I_-$] = 0.

In order for the first derivative of the detected signal in Eq. (11) to be non-zero, two selection rules need to be satisfied:

Selection Rule 1: the error commutator [ρ_n, H_k*(k+1:n)] needs to be non-zero; and

Selection Rule 2: the error commutator [ρ_n, H_k*(k+1:n)] needs to contain an $I\_$ component. This means that ρ_n must contain the coherence order $-1 + p(H_k^*(k+1:n))$, where $p(H_k^*(k+1:n))$ is the coherence order of the operator H_k*(k+1:n) [or one of its coherence orders if H_k*(k+1:n) contains multiple coherences]. Therefore, when computing the error commutator on the right-hand side

(RHS) of Eq. (7), the density matrix ρ_n must include *all coherences* (including non-observable coherences) present at time point n.

The need for the full density matrix ρ_n to be used in Eq. (7) can be understood intuitively in the following terms. The coherences present during the interval k can in general lead to both observable and non-observable coherences in the final density matrix ρ_n. Only the observable coherences in $\partial\rho_n/\partial\theta_k$ contribute to the first derivative of the signal, $\partial S/\partial\theta_k$. However, $\partial\rho_n/\partial\theta_k$ depends on the entire deterministic evolution of the DM from the beginning of interval k to the end of interval n. This evolution is reflected in the past history of the full density matrix ρ_n, which includes its non-observable coherences. The amplitudes of the observable coherences in $\partial\rho_n/\partial\theta_k$ are therefore dependent on the full matrix ρ_n, and non-observable coherences of ρ_n must be taken into account when computing the error commutator $[\rho_n, H_k^*(k{+}1{:}n)]$.

Phase cycling. Equations (7) and (9) are especially useful when considering the behaviour of errors under phase cycling. Two cases are possible when treating the error resulting from variation of the generalised time θ_k:
1) If θ_k is an RF pulse, the phase cycle may apply to the interval k. In this case, the derivative $\partial\rho_n/\partial\theta_k$ is cycled with respect to the phase of H_k;
2) The phase cycling may be performed on an RF pulse m distinct from θ_k: $m \neq k$. In this case the interval θ_k need not be an RF pulse, and $\partial\rho_n/\partial\theta_k$ needs to be phase-cycled with respect to H_m rather than H_k.

In the following, we consider these two cases separately.

Phase cycling on the mis-set RF pulse. Suppose that the RF pulse θ_k and the receiver are phase cycled with the phase increments $\Delta\phi_k$ and $\Delta\phi_R$, respectively. Then only the coherence transfer pathways (CTPs) satisfying the condition $\Delta p_k\,\Delta\phi_k + \Delta\phi_R = 0$ survive the phase cycle (where Δp_k is the change of the coherence order in the given CTP during t_k) [3]. Phase cycling can therefore be expected to restrict the number of the CTPs contributing to signal error (the number of error pathways).

In Appendix A we consider the behaviour of the *first derivative* of the signal under phase cycling and identify the CTPs that contribute to $\partial S/\partial\theta_k$ phase-cycled on the RF pulse θ_k. In the absence

of phase cycling the error commutator $[\rho_n, H_k^*(k{+}1{:}n)]$ has to take into account the full final density matrix ρ_n. As seen from Appendix A, phase-cycling allows the components of ρ_n arising from certain CTPs to be excluded from consideration:

Selection Rule 3: Only the CTPs satisfying the condition $\Delta\phi_R = \Delta\phi_k\,(1 - \Delta p_k) + 2\pi j$ [Eq. (37) in Appendix A] make a non-zero contribution to the first derivative of the phase-cycled signal;

Selection Rule 4: the contributions to the first derivative of the signal from the CTPs selected by the phase cycle (which satisfy the condition $\Delta\phi_R = -\Delta p_k\,\Delta\phi_k$) are cancelled out by the phase cycle.

Besides Selection Rules 3 and 4, selection rules 1 and 2 introduced above apply. Rules 1 and 2 are independent of phase cycling: they must be satisfied in order for $\partial S/\partial\theta_k$ to be non-0 prior to any phase cycling. Application of these results is illustrated in the Results and Discussion section using the example of the two-pulse magnitude COSY experiment.

Phase cycling on a pulse not misset. The case of phase cycling on an RF pulse distinct from the misset generalised time θ_k is considered in Appendix B. The problem of finding the phase-cycled derivative of the signal can in this case be reduced to calculating the average *reverse-transformed observable operator*, $I_-^{*+}(n{:}k{+}1)_{PC}$, given by Eq. (45) in Appendix B. The derivative of the phase-cycled signal can be calculated according to Eq. (46) in Appendix B. Application of these results is illustrated in the Results and Discussion section using the example of the three-pulse DQF COSY experiment.

Pulse phase errors. The RF evolution operator describing the RF pulse of phase ϕ has the form:

$$U = e^{i\theta_k(\cos\phi\cdot I_x + \sin\phi\cdot I_y)} = e^{iH_\phi\theta_k} \tag{12}$$

Consider the effect of mis-setting the phase ϕ. Unlike θ_k, ϕ is not a generalised timing parameter. Therefore, the differentiation of ρ_n with respect to ϕ differs from the approach used to derive Eqs. (7) and (9). Nevertheless, it is convenient to proceed in a way similar to Eq. (4) and represent the derivative of the DM in the form $U_n^+...(-iR_k)U_k^+...U_1^+\rho_0U_1...U_n + U_n^+...U_1^+\rho_0U_1...U_k(iR_k)...U_n$. The appropriate form of the operator R_k can be found by computing the explicit derivative $\partial U/\partial\phi$ in the matrix form and multiplying it on the left by U^{-1}:

$$\frac{\partial U}{\partial \phi} = e^{iH_\phi \theta_k} \cdot [-i \sin\theta_k \sin\phi \cdot I_x + i \sin\theta_k \cos\phi \cdot I_y + 2i \sin^2 \frac{\theta_k}{2} \cdot I_z]$$
$$\frac{\partial U^+}{\partial \phi} = [i \sin\theta_k \sin\phi \cdot I_x - i \sin\theta_k \cos\phi \cdot I_y - 2i \sin^2 \frac{\theta_k}{2} \cdot I_z] \cdot e^{-iH_\phi \theta_k} \quad (13)$$

The derivative of the DM can therefore be represented in a form of Eq. (7), but with a different error interrogation operator:

$$\frac{d\rho_n}{d\phi_k} = i \cdot [\rho_n, U_n^+ ... U_{k+1}^+ \cdot R_k \cdot U_{k+1} ... U_n] = i \cdot [\rho_n, R_k^*(k+1:n)] \quad (14)$$

where the error interrogation operator R_k is given by

$$R_k = -i \sin\theta_k \cdot [I_z, H_{k\phi}] + 2 \sin^2 \frac{\theta_k}{2} I_z \quad (15)$$

Equations (13) – (15) hold for S = ½ as well as higher spins. Equation (14) can be manipulated in the same ways as Eq. (7), and the derivative $d\rho_n/d\phi$ can be expressed via ρ_0 [analogous to Eq. (9)] or ρ_k [analogous to Eq. (33)]. This approach is also applicable to systems of coupled spins provided that the RF pulses are short so that the coupling can be assumed to be "switched off" during the RF pulse. Application of these results is illustrated in the Results and Discussion section using the example of the Jeener-Broekaert experiment.

Resonance offset errors. A similar approach can be used to evaluate the errors resulting from a resonance offset. For an RF excitation pulse of phase ϕ, amplitude ω_1 and resonance offset $\Delta\omega$, the rotating-frame RF excitation Hamiltonian is given by

$$H_k = H_k^{RF}(\phi) + H_k^z(\Delta\omega) = \omega_1 \cdot (\cos\phi \cdot I_x + \sin\phi \cdot I_y) + \Delta\omega \cdot I_z \quad (16)$$

Following the steps leading to Eqs. (13) – (15), we obtain the error interrogation operator valid for $(\Delta\omega/\omega_1)^2 << 1$:

$$R_k = \frac{2i}{\omega_1} \sin^2\left(\frac{\omega_1 t_k}{2}\right) \cdot [I_z, H_k^{RF}] + \frac{1}{\omega_1} \sin(\omega_1 t_k) \cdot I_z \quad (17)$$

where t_k is the physical duration of the RF pulse. In Results and Discussion we present an analysis of the effect of phase cycling on off-resonance errors in the Spin Echo pulse sequence.

Higher-order derivatives. The derivation of the second-order derivative of the final DM is presented in Appendix C. Generalising that derivation, the z-th derivative of ρ_n with respect to θ_k is easily obtained:

$$\frac{d^z \rho_n}{d\,\theta_k^z} = i^z \left[\left[\left[\rho_n, H_k^*(k+1:n)\right], H_k^*(k+1:n)\right], \ldots H_k^*(k+1:n)\right] \tag{18}$$

where the commutator has the depth z. Two basic cases can be distinguished here:

1) The error commutator $[\rho_n, H_k^*(k+1:n)]$ in Eq. (18) is an identical zero. This situation can arise when, down to a constant multiplier, ρ_n equals $H_k^*(k+1:n)$, any power of $H_k^*(k+1:n)$, or a linear combination thereof. In this case, the derivatives of the detected signal $\partial^m S/\partial\theta_k^m$ are equal to zero for all $m \geq 1$, and the signal is completely insensitive to θ_k. [We note that the case $H_k^*(k+1:n) = 0$ is not physically possible because the unitary transformation in Eq. (8) preserves the determinant of H_k.]

2) The error commutator $[\rho_n, H_k^*(k+1:n)]$ and $\partial\rho_n/\partial\theta_k$ are not identical zeros. In this case, all higher derivatives of the DM, $\partial^m\rho_n/\partial\theta_k^m$, are generally non-zero. The derivatives of the observed signal are determined by the coherence orders present in the respective commutators: e.g., if the m-th-order commutator does not contain any coherences of the order −1, then $\partial^m S/\partial\theta_k^m = 0$. This does not preclude the signal derivatives of other orders from being non-zero, provided that the respective commutators contain coherences of the order −1.

Degenerate timing parameters. A generalised timing parameter shared by several intervals in a pulse sequence may be mis-set equally in the intervals concerned. This situation arises very commonly in NMR spectroscopy: e.g., when the durations of hard RF pulses are linked to the calibrated duration of the $\pi/2$ pulse, or when the durations of evolution delays are set based on the value of a coupling constant. For several generalised times sharing a common value, $\theta_{k1} = \theta_{k2} = \ldots = \theta_{kq} = \theta$, it is easily shown that the cumulative derivative of the DM with respect to θ is given by:

$$\frac{d\rho_n}{d\,\theta} = \sum_{i=1}^{q} \left.\frac{\partial\rho_n}{\partial\,\theta_{k_i}}\right|_{\theta_{k_i}=\theta} \tag{19}$$

It should be noted that the summation terms on the RHS of Eq. (19) are generally not equal, even if the Hamiltonians H_i are. The error interrogation operator $H_k^*(k{+}1{:}n)$ is the result of the unitary transformation $U_{k+1}...U_n$, while the operator $H_m^*(m{+}1{:}n)$ is obtained from the unitary transformation $U_{m+1}...U_n$. If these two unitary transformations are not equal, then the transformed operators $H_k^*(k{+}1{:}n)$ and $H_m^*(m{+}1{:}n)$ are not identical, and each term in the summation must be computed individually.

Higher-order derivatives of ρ_n with respect to a degenerate generalised time θ, $\partial^z\rho_n/\partial\theta^z$, can be expressed via multiple commutators similar to that shown in Eq. (18). For $z \geq 2$, the respective summation contains diagonal terms of the type $[[[\rho_n, H_i^*], H_i^*],...]$ as well as cross-terms $[[[\rho_n, H_i^*], H_j^*],...]$. Because of the cross-terms, the cumulative higher-order derivatives $\partial^z\rho_n/\partial\theta^z$ are not simple sums of the q terms $\partial^z\rho_n/\partial\theta_k{}^z$ representing the derivatives with respect to the individual parameters [as was the case in Eq. (19)]. For the case of M degenerate generalised times $\{\theta_{k1}, \theta_{k2},..., \theta_{kM}\}$ and derivative of the order z, there are M^z possible commutators of depth z. Of these, $C^{M-1}{}_{z+M-1} = (z{+}M{-}1)!/z!(M{-}1)!$ commutators are distinct. The expression for the z-th derivative is given by the following summation of depth z:

$$\frac{d^{(z)}\rho_n}{d\,\theta^z} = i^z \sum_{i=k_1}^{k_M}\sum_{j=i}^{k_M}\cdots\sum_{m=l}^{k_M}\binom{M}{p_{k_1}, p_{k_2}, \ldots, p_{k_M}}\left[\left[\left[\rho_n,\, H_i^*\right],\, H_j^*\right],\ldots H_m^*\right] \tag{20}$$

where p_{k1}, p_{k2}, etc. are the number of times the parameters k_1, k_2,... occur in the respective z-fold commutator. The coefficients in front of the commutators are multinomial coefficients:

$$\binom{M}{p_{k_1}, p_{k_2}, \ldots, p_{k_M}} = \frac{M!}{p_{k_1}!\; p_{k_2}!\ldots\; p_{k_M}!} \tag{21}$$

which have the meaning of the number of distinct permutations of the set of indices of length z, $\{i, j,..., m\}$. The treatment of degenerate derivatives is illustrated in Results and Discussion using the example of Carr – Purcell and Carr – Purcell – Meiboom – Gill experiments.

NUMERICAL SIMULATIONS

The analytic predictions of the error commutator formalism were verified using numerical DM simulations. Several NMR pulse sequences were investigated, as described in Results and Discussion: Carr – Purcell [4] and Carr – Purcell – Meiboom – Gill [5]; spin echo [6]; two-pulse (magnitude) COSY [7]; double-quantum filtered three-pulse COSY [8]; and the Jeener-Broekaert [9] experiments.

For each pulse sequence investigated, two types of simulations were performed:
1) Conventional DM simulations based on the standard NMR DM formalism [3,10,11]. In these simulations, the parameter varied was kept in the symbolic form; all other simulation parameters were given numerical values. The observed signal was calculated as $S = Tr[I_{-}^{+} \cdot \rho_n]$. The detected signal S was therefore a function of the symbolic parameter varied. The derivatives of the signal were computed by explicit differentiation.
2) Simulations of the DM and signal errors based on the error commutator formalism. In these simulations, the standard DM formalism was augmented to compute the error interrogation operators [Eqs. (8) and (15)], reverse-transformed observable operators [Eq. (44)] and error commutators [Eqs. (7), (9), (34), (18) and (14)], as required. This, in turn, was used to compute the first and higher derivatives of the DM and the observed signal with respect to the mis-set parameter. The derivatives of the observed signal were calculated according to Eq. (11) and the equivalent expressions for the higher derivatives. In the ECF, the information about signal variation under mis-set parameters is contained in the error commutators computed using the ideal pulse sequence parameters; therefore, ECF simulations allowed all-numerical parameters to be used in the evaluation of derivatives. Analytic expressions for error interrogation operators, error commutators and derivatives were also computed in selected cases in order to illustrate the compactness of the ECF analysis.

The DM and signal derivatives obtained using the error commutator formalism and the conventional DM simulations were compared; the two sets of results were found to be always identical within the rounding error.

RESULTS AND DISCUSSION

Execution of NMR experiments usually requires that the pulse sequence parameters be set to their "correct" values. This includes, for example, calibration of the flip angle of RF pulses, or setting evolution delays on the basis of a coupling constant (e.g., $1/2J$ in the case of scalar couplings). However, it is usually not possible to set pulse sequence parameters to their exact ideal values, and the acquired signal can contain systematic errors arising either from unwanted CTPs or from an incomplete conversion between a set of coherences. Some of the general approaches to dealing with this problem include CTP selection by means of phase cycling [12-15] or pulsed field gradients [3,16,17] and the design of robust pulses [18-25] or pulse sequences [26-34]. While these approaches significantly alleviate the effects of non-ideality of pulse sequences, they usually cannot eliminate the errors altogether. It is therefore useful to be able to analyse the sensitivity of a pulse sequence to variations of its parameters.

The Error Commutator Formalism (ECF) is an intuitive and easy-to-use tool for such analysis. Here we present an ECF analysis of several NMR experiments in order to illustrate the approach described in the Theory section. We follow the standard NMR sign conventions [35,36]:

$$\begin{aligned} e^{i\theta I_\alpha} I_\beta e^{-i\theta I_\alpha} &= I_\beta \cos\theta - I_\gamma \sin\theta \\ I_x &\xrightarrow{\omega_0 t I_z} I_x \cos(\omega_0 - \omega_{RF})t - I_y \sin(\omega_0 - \omega_{RF})t \\ I_z &\xrightarrow{\theta I_x} I_z \cos\theta + I_y \sin\theta \\ I_{1x} &\xrightarrow{\pi J t \cdot 2 I_{1z} I_{2z}} I_{1x} \cos\pi J t + 2 I_{1y} I_{2z} \sin\pi J t \end{aligned} \qquad (22)$$

where both θ and ω_0 are taken as positive quantities: $\omega_0 = +\gamma\hbar B_0$ and $\theta = +\gamma\hbar B_1 t$; ω_{RF} is the precession frequency of the rotating frame; and the permutation $\alpha \rightarrow \beta$ is "clockwise".

Mis-set RF pulse durations: Carr-Purcell vs Carr-Purcell-Meiboom-Gill experiment. In order to demonstrate the basics of the error commutator formalism, we consider two well-understood experiments: Carr-Purcell (CP) and Carr-Purcell-Meiboom-Gill (CPMG). The two experiments are closely related and essentially share the same pulse sequence (shown in Fig. 2); the difference between them is in the phase of the refocusing π RF pulses: $\alpha = x$ for CP and $\alpha = y$ for CPMG. A well-known feature of CPMG is the relative insensitivity of its even echoes to

miscalibration of the refocusing π RF pulse. Here we demonstrate the basis for the relative robustness of CPMG using a single spin-1/2 as an example.

The Hamiltonians effective during different intervals are shown in Table 1, along with the ideal DM at the top of the echoes. Transforming the operator I_x, we obtain the error interrogation operator of the k-th refocusing pulse at the n-th CP echo:

$$H_k^*(n) = -I_x \cos(\omega\tau) + (-1)^{n-k} I_y \sin(\omega\tau) \tag{23}$$

The equivalent error interrogation operator for the CPMG sequence is

$$H_k^*(n) = -(-1)^{n-k} I_x \sin(\omega\tau) - I_y \cos(\omega\tau) \tag{24}$$

Assuming that the pulse sequence contains n refocusing π pulses of equal durations, the duration of the refocusing pulse can be considered an n-fold-degenerate generalised time. At the n-th echo there will be n error interrogation operators corresponding to pulses from 1 to n; these operators are given by Eqs. (23) (CP) and (24) (CPMG). Cumulative first-order derivatives of the DM can be calculated using Eq. (19). Cumulative higher derivatives are calculated using Eq. (20). The z-th derivative includes $((z+n-1)!/z!(n-1)! - n)$ cross-terms as well as n diagonal terms. Analytic expressions for the cumulative first- and second-order DM derivatives at the n-th echo are summarised in Table 2. The expressions for $z \geq 3$ are also obtained easily in a compact form but not shown here for the sake of brevity. It is worth noting that non-zero derivatives of the DM do not always correspond to non-zero derivatives of the observable signal. For instance, the first-order DM derivatives in both CP and CPMG contain no transverse components and, on their own, do not result in signal errors. However, the error commutators $[\rho_n, H_k^*(k+1{:}n)] \propto I_z$ lead to I_x and I_y terms in the second-order commutators; as a result, the non-observable first-order DM errors are manifest in higher-order derivatives of the observable signal.

Two significant points are evident from Table 2. First, the CPMG errors grow more slowly with n than the CP errors. The first derivative of the CP echo grows linearly with n. The corresponding CPMG derivative is constant for all odd echoes and never exceeds the order-of-magnitude of the smallest CP derivative. The second-order derivative grows as $O(n^2)$ for CP echoes but only as $O(n)$ for CPMG echoes. Second, at even echoes certain terms in the CPMG

derivatives turn exactly to zero: namely, the entire first-order derivative and the I_y term of the second-order derivative. Therefore, the detected (transverse) magnetisation at even CPMG echoes is subject to errors of the order of $n(\delta\theta)^2$, which can be expected to be significantly smaller than the CP errors under equivalent conditions. Figure 3 shows representative plots of the I_x, I_y and I_z components of the DM errors in the two experiments as a function of n. The errors plotted were obtained using the error commutator formalism. For comparison, "exact" errors were also computed by explicitly simulating the evolution of the DM under non-ideal refocusing pulses (not shown). For the situation considered ($\omega\tau = 2$, $\delta\theta = -\pi/18$, spin relaxation neglected), the ECF errors converged rapidly: for both CP and CPMG, the ECF errors matched the "exact" errors to within 4%, 0.1% and 0.001% of M_0 upon the inclusion of the first two, four and six derivatives, respectively.

Figure 3 demonstrates the well-known robustness of the CPMG pulse sequence, compared to CP, with respect to miscalibration of the refocusing π pulse. But more importantly, the ECF-derived expressions shown in Eqs. (23) and (24) and Table 2 enable a detailed understanding of how the errors arising from individual RF pulses propagate through the pulse sequence. The intuitive and general nature of ECF can be used to advantage in the analysis of performance of NMR pulse sequences and pulse sequence design.

One more advantageous feature of the ECF is worth emphasising. In order to investigate the sensitivity of NMR experiments with respect to non-ideal RF pulses, only the DM corresponding to the *ideal* ($\pi/2$ and π) RF pulses needs to be computed. (We note that this also applies to Kuprov and Rodgers' approach [1].) The DM for $\theta \neq \pi$ need not be computed in order to obtain the derivatives shown in Table 2 because these derivatives are implicit in the ideal ($\theta = \pi$) density matrix. This can provide a significant computational advantage (compared to finite-difference methods) when the ECF is used for complicated pulse sequences.

Spin-echo pulse sequence: off-resonance errors under phase cycling. Equation (17) can be used to analyse the phase-cycling behaviour of errors resulting from off-resonance RF pulses. Here we consider the spin-echo experiment (Fig. 4) and evaluate the DM errors arising from an off-resonance refocusing π pulse. The errors are computed at the top of the echo ($t_4 = t_2$). For the sake of simplicity, a single spin-1/2 is considered; the phase cycle used is the four-step EXORCYCLE [12]. Table 3 shows the ideal DM at the top of the echo (the end of interval t_4), as

well as the first two derivatives of the DM with respect to the resonance offset, $\Delta\omega$. The derivatives include the effects of off-resonance evolution during the echo time as well as off-resonance evolution during the π pulse *per se*. It is noteworthy that the steps of the phase cycle are not equivalent in terms of sensitivity to $\Delta\omega$: the first-order error of the DM is zero in steps 1 and 3 ($\phi = \pm x$) but non-zero in steps 2 and 4 ($\phi = \pm y$). The first-order error contains no transverse coherences and therefore does not affect the signal detected at the echo. However, it can be of consequence when the spin-echo sequence is used to prepare magnetisation for further manipulation (as is done, e.g., in INEPT). The ECF analysis can therefore inform the choice of RF pulse phases in complex NMR pulse sequences. The first-order error is cancelled out in the two-step phase cycle (π_y, π_{-y}) (column 6 of Table 3). The second-order error completely survives both the two-step and the four-step EXORCYCLE (Table 3, columns 6 and 7, respectively).

Spin-echo pulse sequence: phase errors of the π pulse under phase cycling. Here we analyse the DM errors arising from a phase error of the refocusing π pulse in the spin-echo experiment. The setup of the experiment and the phase cycle are as described in the previous paragraph ($t_4 = t_2$; single spin-1/2; four-step EXORCYCLE phase cycle). The general phase-cycling behaviour of the signal errors is presented in Eq. (41) in Appendix A. Because the RF pulse in question is a π pulse, only the second term of Eq. (41) contributes to the error even before phase cycling. The results are presented in Table 4. The first-order error of the acquired signal is identical in each step of the four-step EXORCYCLE. This corresponds to a simple phasing error of the acquired echo signal resulting from an effective phase offset of the rotating frame. The error-free signal in this case can be reconstructed by zeroth- and first-order rephasing of the frequency domain data.

Two-pulse COSY experiment. Consider the two-pulse COSY experiment ("magnitude COSY", Fig. 5) [7] as an example of the effect of phase-cycling the mis-set RF pulse. For the sake of simplicity, consider the two-step phase cycle: the phases of the first RF pulse and the receiver are kept at $+x$; the phase of the second RF pulse is alternated between $+x$ and $-x$ [8]. We assume a strongly coupled homonuclear system of two spins-1/2 and are interested in the derivative of the signal with respect to the duration of the mis-set pulse: $\partial S/\partial\theta_3$.

The dimensionless Hamiltonians effective during different intervals of the pulse sequence are:

$$
\begin{aligned}
H_1 &= \left(I_{1x} + I_{2x}\right) \\
H_3 &= \pm\left(I_{1x} + I_{2x}\right) \\
H_2 = H_4 &= -\left(I_{1z} + I_{2z}\right) + \frac{\pi J}{\omega_0}\left(I_{1+}I_{2-} + I_{1-}I_{2+} + 2I_{1z}I_{2z}\right)
\end{aligned}
\tag{25}
$$

A symbolic analysis provides insights into the behaviour of signal errors under phase cycling. It also enables the identification of the specific components of the DM contributing to the error of the detected signal. The appropriate error interrogation operator has the form

$$
H_3^*\left(4:4\right) = e^{-i\left(AI_{1z} + BI_{2z} + CI_{1z}I_{2z} + D(I_{1+}I_{2-} + I_{1-}I_{2+})\right)}\left(\pm\left(I_{1x} + I_{2x}\right)\right)e^{i\left(AI_{1z} + BI_{2z} + CI_{1z}I_{2z} + D(I_{1+}I_{2-} + I_{1-}I_{2+})\right)} \tag{26}
$$

It is clear that H_3*(4:4) contains only coherences of the orders +1 and −1. This enables us to restrict, using the following reasoning, the number of CTPs that have the capacity to contribute to signal error:

1) According to Eq. (36), the operator $U_4^+[\rho_3, H_3]U_4$ needs to contain terms with coherence order $p = -1$ in order for the misset θ_3 to lead to a signal error;

2) But the transformation U_4 preserves the coherence order; therefore, it is the operator $[\rho_3, H_3]$ that needs to contain terms with $p = -1$;

3) $p([\rho_3, H_3]) = p(\rho_3) + p(H_3)$. Because $p(\rho_3) = p(\rho_4)$, only the components of ρ_4 that satisfy the condition $p(\rho_4) + p(H_3) = -1$ lead to signal error;

4) As seen from Eq. (26), $p(H_3) = \pm 1$;

5) Therefore, even prior to phase cycling, the only components of ρ_4 capable of contributing to signal error are those with the coherence orders $p_4 = -1 \pm 1 = 0$ or -2.

Error contributions that survive the phase cycle can be identified using Eq. (37). Only the CTPs with $\Delta p_3 = 1$, -1 and -3 lead to signal errors that survive the phase cycle (where Δp_3 is the coherence order change during the second RF pulse). These CTPs are shown in Fig. 5b as dotted lines.

We have analysed the contributions of individual CTPs to the signal and its error using both the ECF [Eq. (7)] and explicit density-matrix simulations with a symbolic θ_3. A summary of the results is presented in Table 5. The main observations are as follows:

1) Of the possible 3 x 5 = 15 CTPs, only four contributed to the signal error: (−1, −2), (−1, 0), (1, −2) and (1, 0). These CTPs (shown as the dotted lines in Fig. 5b) satisfy the selection rules $p_4 = 0$ or −2 and $\Delta p_3 = 1, -1$ and −3 discussed above;
2) The contributions to the signal error from the two selected CTPs, (−1, −1) and (1, −1), were zero in each step of the phase cycle. This is consistent with the selection rule for p_4;
3) The phases of the errors arising from each of the "dotted" CTPs of Fig. 5b were identical in the two steps of the phase cycle, and a given CTP therefore contributed identical amounts to the signal error in steps 1 and 2. This is consistent with Eq. (37);
4) Using explicit DM formalism, analytic signal derivatives were computed for each of the selected CTPs, (−1, −1) and (1, −1). The derivative of the signal filtered through (−1, −1) was identically equal to the sum of the ECF-computed derivatives contributed by the CTPs (−1, −2) and (−1, 0). Likewise, the derivative of the signal filtered through (1, −1) was identical to the sum of ECF-computed derivatives from (1, −2) and (1, 0). Generally, the derivative of the observed signal filtered through a coherence order p_k is given by the error commutator of Eq. (7) where ρ_n includes the contributions (both observable and non-observable) from all the CTPs containing p_k.

Double-quantum filtered COSY. We now consider the double quantum-filtered (DQF) COSY experiment (Fig. 6) [8] as an example of phase-cycling on an RF pulse different from the pulse mis-set. We assume a homonuclear AX system of two spins-1/2 and use the 4-step phase cycle shown in Table 6.

First, let us show that the derivative of the phase-cycled signal with respect to the duration of the second RF pulse, $dS_{PC}/d\theta_3$, is zero. This can be shown analytically by phase-cycling the reverse-transformed observable operator given by Eq. (44), Appendix B. This approach takes advantage of the fact that all the phase cycling here occurs after the pulse mis-set (interval t_3). Therefore, the error of the phase-cycled detected signal can be calculated using Eq. (46), where the commutator $[\rho_3, H_3]$ is left unchanged in all steps of the phase cycle, while the reverse-transformed observable operator $I_+^*(5{:}4)$ is phase-cycled.

It is easily shown that the phase-cycled observable operator is given by

$$I_+^*(5:4)_{PC} = AI_{1+}I_{2+} - AI_{1-}I_{2-} \tag{27}$$

where A is a complex coefficient dependent on t_5, J and ω_i. The Hamiltonian H_3 (identical in each step of the phase cycle) has the form

$$\hat{H}_3 = I_{1x} + I_{2x} \tag{28}$$

The form of the (non-transformed) density matrix ρ_3 can be gleaned from the following considerations:

1) $\mathrm{Tr}[\rho_3] = 0$;

2) Because ρ_3 is Hermitian, the amplitudes of coherences that are Hermitian conjugates of each other must be complex-conjugates of each other. That is, if the amplitude of $I_{1+}I_{2-}$ in ρ_3 is B, then the amplitude of $I_{1-}I_{2+}$ is B*, etc.;

3) The second RF pulse creates the Cartesian coherences $I_{1z}I_{2y}$, $I_{1y}I_{2z}$ with real amplitudes and no coherences $I_{1z}I_{2x}$, $I_{1x}I_{2z}$. Because $I_y = (I_+ - I_-)/2i$, the amplitudes of the antiphase single-quantum (SQ) coherences $I_{1z}I_{2\pm}$ and $I_{1\pm}I_{2z}$ in ρ_3 must be purely imaginary.

Only DQ terms of the commutator $[\rho_3, H_3]$ contribute to error of the phase-cycled signal because the phase-cycled observable operator $I_+^*(5{:}4)$ [Eq. (27)] contains only DQ coherences. Taking into account the restrictions on the form of ρ_3 discussed in the previous paragraph, the DQ part of the commutator has the form:

$$[\rho_3, H_3]_{DQ} = i\,C\left(I_{1+}I_{2+} + I_{1-}I_{2-}\right) \tag{29}$$

where C is a real coefficient. The error of the phase-cycled observed signal is easily seen to be zero because A is complex and C is real:

$$\left(\frac{d\,S}{d\,\theta_3}\right)_{PC} = i \cdot Tr\left[A \cdot (I_{1+}I_{2+} - I_{1-}I_{2-}) \cdot i\,C(I_{1+}I_{2+} + I_{1-}I_{2-})\right] = 0 \tag{30}$$

Therefore, the phase cycle used eliminates the first-order signal error arising from variation of the second $\pi/2$ RF pulse. We also note that the signal errors in the individual steps of the phase cycle are not necessarily zero because $I_+^*(5{:}4)$ is not restricted to DQ coherences in individual steps of the phase cycle.

Similar error analysis can be carried out using the original approach, where the error interrogation operator is forward-transformed according to Eq. (8). In this approach, the phase cycling affects both the observable operator (which is phase-cycled according to Table 6) and the transformed error interrogation operator (which varies between the steps of the phase cycle because the unitary operator U_4 depends on the phase-cycled H_4). This analysis also shows that the phase-cycled $dS/d\theta_3 = 0$. We have carried out this analysis for every individual CTP; the key results are summarised in Table 7. The following additional observations can be made from the CTP-selective error analysis:

1) In steps 1 and 3 of the phase cycle, the error interrogation operator $H_3^*(4{:}5)$ contains only zero-quantum (ZQ) coherences. Consequently, only the CTPs with $p_4 = -1$ contribute to the signal error in these steps. This is consistent with Eq. (11);

2) In steps 2 and 4 the operator $H_3^*(4{:}5)$ contains only SQ coherences: $p[H_3^*(4{:}5)] = \pm 1$. In these steps, only the CTPs with $p_4 = 0$ or -2 contribute to signal error;

3) The signal errors computed using the ECF were verified using explicit DM simulations. In each step of the phase cycle, the total DM-computed signal derivative was equal to the sum of the ECF-computed contributions from all CTPs;

4) The total signal error is non-zero in steps 1 and 3 but zero in steps 2 and 4;

5) The error contributions from the selected CTPs cancel out between steps 1 and 3 and also between steps 2 and 4. Only CTPs that are not selected by the phase cycle contribute a non-zero error to the phase-cycled signal;

6) The total error of the phase-cycled signal (i.e. the sum of the phase-cycled contributions from the individual CTPs) is zero.

The utility of the analysis shown for the two COSY experiments lies in its capacity to identify specific contributions to signal error, or "error coherence transfer pathways". The knowledge of "error CTPs" makes possible the elimination of some of the error contributions and provides general, analytic insights into the behaviour of signal errors under phase cycling. ECF analysis can therefore inform the development of phase cycling schemes aimed at minimising the number of surviving error CTPs. It can also inform the engineering of robust NMR experiments insensitive to RF pulse imperfections.

RF pulse phase errors: the Jeener-Broekaert experiment. The Jeener-Broekaert experiment is used for selective observation of orientationally ordered quadrupolar nuclei [9,37]. Its spin-echo

implementation (Fig. 7) includes a spin-echo block ($\pi/2 - \tau/2 - \pi - \tau/2$) and a ZQ filter (two $\pi/4$ RF pulses, the second of which is phase-cycled according to Table 8). The ZQ filter selects the signal from quadrupolar nuclei in partially aligned environments but suppresses (after the phase cycle) the signal from nuclei in isotropic environments. The perfect selectivity requires that the phases of the $\pi/2$ pulse and the first $\pi/4$ RF pulse be orthogonal. Here, we illustrate the effect of mis-setting the relative phases of these pulses. The relevant DM derivative and the error interrogation operator are given by Eqs. (14) and (15), respectively.

We considered the phase-cycled Jeener-Broekaert signal from an ensemble of single spins-1, of which 60% resided in a partially aligned and the remaining 40% in an isotropic environment. The aligned environment was assumed to be axially symmetric, and its free-evolution spin Hamiltonian was:

$$H = -\omega_0 I_z + \omega_Q \left(3I_z^2 - 2\right) \tag{31}$$

The free-evolution Hamiltonian of the "isotropic" nuclei contained only the Zeeman term:

$$H = -\omega_0 I_z \tag{32}$$

The effect of RF phase errors on the spectra was simulated numerically using both the standard DM formalism and the ECF. The key simulation parameters were: $\omega_0 = 1113$ Hz; $\omega_Q = 2000$ Hz; $t_2 = t_4 = 10$ ms; $T_2 = 6$ ms; dwell time 100 μs; 8192 complex FID points. Figure 8a shows the DM-simulated phase-cycled Jeener-Broekaert spectrum obtained with the perfect RF phases (Table 8). Figure 8b shows the DM-simulated spectrum obtained with a misset phase P3 (0.48π instead of $\pi/2$). Figure 8c is the difference between the spectra 8b and 8a. Figure 8d shows the difference spectrum computed using the error commutator formalism [Eq. (14)]. The latter matches the difference spectrum calculated from explicit density-matrix simulations, providing a validation of the theory presented in "Pulse phase errors" in the Theory section.

General remarks and conclusions. Analytic approaches to evaluation of derivatives of the NMR signal with respect to pulse sequence parameters have been presented in the past [1,38-40]. In a distinct but closely related work in NMR optimal-control theory, Khaneja *et al* calculated the derivatives of the expectation value of an arbitrary target operator with respect to control

amplitudes [34]. An experimental example also exists where the derivative of the NMR signal with respect to a parameter of the pulse sequence was linked to the signal from a second pulse sequence [41]. The error commutator formalism presented here is a simple but powerful approach for analytic evaluation of NMR density matrix derivatives with respect to pulse sequence parameters. It can be applied to any situation amenable either to Density-Matrix or Product-Operator (PO) treatment, provided that spin relaxation and chemical kinetics can be neglected. The calculation of transformed error interrogation operators [Eqs. (8) and (10)] and reverse-transformed observable operators [Eq. (44)] is conceptually identical to calculation of the evolution of the spin density matrix or product operators in NMR pulse sequences. When the PO approximation is appropriate, the transformed error interrogation operators and reverse-transformed observable operators can be computed using the standard PO rules [2].

The calculation of signal errors using the commutator approach imposes little additional cost compared to calculating the evolution of the spin DM for a pulse sequence with the *ideal* RF pulses and delays. Information about signal variation under mis-set pulse sequence parameters is implicitly contained in the density matrix computed for the ideal parameters. The error commutator formalism enables the extraction of this implicit information.

The approach presented is algorithmic and easily amenable to implementation in the form of a programming code. The expressions arising in the ECF are computationally similar to the standard PO or DM formalisms. It is therefore envisaged that error commutator analysis could be incorporated into standard NMR product-operator simulation packages such as POMA [42].

The principal application of this approach envisaged by the authors is the analysis of sensitivity of NMR pulse sequences to variations of the pulse sequence parameters. The “robust” pulse sequences are those in which the lower derivatives of the DM with respect to a perturbed parameter are zero. The error commutator formalism provides for facile identification of such pulse sequences. Its distinct advantage is that it enables error analysis at the level of individual CTPs (“error coherence transfer pathways”), making it possible to analyse individual contributions to the error of the final DM. The error commutator formalism is especially well-suited for the analysis of the behaviour of errors under phase cycling, and it is envisaged that it can become a useful tool in phase cycle design.

A promising generalisation of the error commutator analysis is the use of group theory for the identification of zero and non-zero error contributions. Group theory has been invaluable in quantum chemistry and chemical spectroscopy for identifying selection rules pertaining to molecular-orbital integrals or interactions of molecules with radiation. Its use in the error commutator analysis may simplify the identification of CTPs that make a zero contribution to signal error.

It is also envisaged that the error commutator formalism can become a useful tool in the development of NMR and EPR quantum computing applications, where both precise manipulation of spin qubits and error correction are required.

Acknowledgements. This research was supported by QUT Professional Development Leave funding to K.I.M. and by funding from the Global COE program, International Center for Integration Research and Advanced Education in Material Science, Kyoto University. The authors thank Dr K. Takeda for fruitful discussions and the reviewers for their helpful comments. K.I.M. thanks Mr Chris Bell for contributing to the typesetting of the manuscript.

References

[1] I. Kuprov, C.T. Rodgers, Derivatives of spin dynamics simulations, J. Chem. Phys. 131 (2009) 234108.

[2] O.W. Sorensen, G.W. Eich, M.H. Levitt, G. Bodenhausen, R.R. Ernst, Product operator formalism for the description of NMR pulse experiments, Prog. Nucl. Magn. Reson. Spectrosc. 16 (1983) 163-192.

[3] M.H. Levitt, Spin Dynamics: Basics of Nuclear Magnetic Resonance, John Wiley & Sons, Chichester, 2001.

[4] H.Y. Carr, E.M. Purcell, Effects of diffusion on free precession in nuclear magnetic resonance experiments, Phys. Rev. 94 (1954) 630-638.

[5] S. Meiboom, D. Gill, Modified spin-echo method for measuring nuclear relaxation times, Rev. Sci. Instr. 29 (1958) 688-691.

[6] E.L. Hahn, Spin echoes, Phys. Rev. 80 (1950) 580-594.

[7] J. Jeener, Two-dimensional Fourier transform NMR. Ampere Summer School, Basko Polje, Yugoslavia, 1971.

[8] S. Berger, S. Braun, 200 and More NMR Experiments: A Practical Course, Wiley-VCH, Weinheim, Great Britain, 2004.

[9] J. Jeener, P. Broekaert, Nuclear magnetic resonance in solids - Thermodynamic effects of a pair of RF pulses, Phys. Rev. 157 (1967) 232-240.

[10] K.J. Packer, K.M. Wright, The use of single-spin operator basis sets in the NMR spectroscopy of scalar-coupled spin systems, Mol. Phys. 50 (1983) 797-813.

[11] P.J. Hore, S. Wimperis, J.A. Jones, NMR, The Toolkit, Oxford University Press, Oxford; New York, 2000.

[12] G. Bodenhausen, R. Freeman, D.L. Turner, Suppression of artifacts in two-dimensional J spectroscopy, J. Magn. Reson. 27 (1977) 511-514.

[13] A.D. Bain, Coherence levels and coherence pathways in NMR. A simple way to design phase cycling procedures, J. Magn. Reson. 56 (1984) 418-427.

[14] D.L. Turner, Phase Cycling, in: D.M. Grant, R.K. Harris (Eds.), Encyclopedia of Nuclear Magnetic Resonance, Wiley, New York, 1996, pp. 3585-3592.

[15] C.E. Hughes, M. Carravetta, M.H. Levitt, Some conjectures for cogwheel phase cycling, J. Magn. Reson. 167 (2004) 259-265.

[16] A. Jerschow, N. Müller, Convection compensation in gradient enhanced nuclear magnetic resonance spectroscopy, J. Magn. Reson. 132 (1998) 13-18.

[17] K.I. Momot, P.W. Kuchel, Convection-compensating diffusion experiments with phase-sensitive double-quantum filtering, J. Magn. Reson. 174 (2005) 229-236.

[18] R. Freeman, Spin Choreography: Basic Steps in High Resolution NMR, Spektrum, Oxford, 1997.

[19] C. Counsell, M.H. Levitt, R.R. Ernst, Analytical theory of composite pulses, J. Magn. Reson. 63 (1985) 133-141.

[20] M.H. Levitt, Composite pulses, Prog. Nucl. Magn. Reson. Spectrosc. 18 (1986) 61-122.

[21] L. Emsley, G. Bodenhausen, Optimization of shaped selective pulses for NMR using a quaternion description of their overall propagators, J. Magn. Reson. 97 (1992) 135-148.

[22] S. Wimperis, Broad-band, narrow-band, and passband composite pulses for use in advanced NMR experiments, J. Magn. Reson. A 109 (1994) 221-231.

[23] H.T. Hu, A.J. Shaka, Composite pulsed field gradients with refocused chemical shifts and short recovery time, J. Magn. Reson. 136 (1999) 54-62.

[24] K. Kobzar, B. Luy, N. Khaneja, S.J. Glaser, Pattern pulses: design of arbitrary excitation profiles as a function of pulse amplitude and offset, J. Magn. Reson. 173 (2005) 229-235.

[25] M. Braun, S.J. Glaser, Cooperative pulses, J. Magn. Reson. 207 (2010) 114-123.

[26] T.J. Norwood, An eddy-current-independent multiple-quantum method for measuring the diffusion of coupled spins, J. Magn. Reson. 99 (1992) 208-213.

[27] K. Takegoshi, C.A. McDowell, A "magic echo" pulse sequence for the high-resolution NMR spectra of abundant spins in solids, Chem. Phys. Lett. 116 (1985) 100-104.

[28] K. Takegoshi, K. Ogura, K. Hikichi, A perfect spin echo in a weakly homonuclear J-coupled two spin-1/2 system, J. Magn. Reson. 84 (1989) 611-615.

[29] K.I. Momot, P.W. Kuchel, Convection-compensating PGSE experiment incorporating excitation-sculpting water suppression (CONVEX), J. Magn. Reson. 169 (2004) 92-101.

[30] K.I. Momot, P.W. Kuchel, PFG NMR diffusion experiments for complex systems, Concepts Magn. Reson. 28A (2006) 249-269.

[31] T.L. Hwang, A.J. Shaka, Water suppression that works. Excitation sculpting using arbitrary waveforms and pulsed field gradients, J. Magn. Reson. A 112 (1995) 275-279.

[32] A.M. Torres, T.T. Nakashima, R.E.D. McClung, D.R. Muhandiram, Improvement of INADEQUATE using compensated delays and pulses, J. Magn. Reson. 99 (1992) 99-117.

[33] A.M. Torres, G. Zheng, W.S. Price, J-compensated PGSE: an improved NMR diffusion experiment with fewer phase distortions, Magn. Reson. Chem. 48 (2010) 129-133.

[34] N. Khaneja, T. Reiss, C. Kehlet, T. Schulte-Herbruggen, S.J. Glaser, Optimal control of coupled spin dynamics: design of NMR pulse sequences by gradient ascent algorithms, J. Magn. Reson. 172 (2005) 296-305.

[35] C.P. Slichter, Principles of Magnetic Resonance, Springer-Verlag, Berlin; New York, 1990.

[36] B.C. Gerstein, Rudimentary NMR: The Classical Picture, in: D.M. Grant, R.K. Harris (Eds.), Encyclopedia of Nuclear Magnetic Resonance, Wiley, New York, 1996, pp. 4197-4204.

[37] R. Kemp-Harper, S. Wimperis, Detection of the interaction of sodium ions with ordered structures in biological systems. Use of the Jeener-Broekaert experiment, J. Magn. Reson. B 102 (1993) 326-331.

[38] D.G. Cory, A simple, efficient algorithm for determining the toggling-frame states of multiple-pulse cycles, J. Magn. Reson. 96 (1992) 171-173.

[39] A.J. Benesi, Series expansion of propagators, J. Magn. Reson. A 103 (1993) 230-233.

[40] A. Jerschow, Nonideal rotations in nuclear magnetic resonance: Estimation of coherence transfer leakage, J. Chem. Phys. 113 (2000) 979-986.

[41] O.W. Sorensen, Linking NMR pulse sequences: Derivative relation between the responses of two pulse sequences, J. Magn. Reson. 174 (2005) 335-337.

[42] P. Guntert, N. Schaefer, G. Otting, K. Wuthrich, POMA - A complete Mathematica implementation of the NMR product-operator formalism, J. Magn. Reson. A 101 (1993) 103-105.

[43] U. Piantini, O.W. Sorensen, R.R. Ernst, Multiple quantum filters for elucidating NMR coupling networks, J. Am. Chem. Soc. 104 (1982) 6800-6801.

[44] A.J. Shaka, R. Freeman, Simplification of NMR spectra by filtration through multiple-quantum coherence, J. Magn. Reson. 51 (1983) 169-173.

Appendix A: The effect of phase cycling on the errors arising from a mis-set RF pulse

Consider the effect of phase-cycling the misset RF pulse (θ_k) on the error of the detected signal ($\partial S/\partial\theta_k$). In order to find the phase-cycled $\partial\rho_n/\partial\theta_k$, it is convenient to modify Eq. (7):

$$\begin{aligned}\frac{\partial\rho_n}{\partial\theta_k} &= i[\rho_n, H_k^*(k+1:n)] = i[U_n^+ \ldots U_{k+1}^+ \cdot \rho_k \cdot U_{k+1} \ldots U_n,\ U_n^+ \ldots U_{k+1}^+ \cdot H_k \cdot U_{k+1} \ldots U_n] \\ &= i \cdot U_n^+ \ldots U_{k+1}^+ \cdot [\rho_k, H_k] \cdot U_{k+1} \ldots U_n\end{aligned} \tag{33}$$

If the phase cycling is performed solely on θ_k, then none of the unitary operators U_{k+1} ... U_n are phase-cycled. Therefore, direct effects of the phase cycle are confined to the commutator $[\rho_k, H_k]$ in Eq. (33). The phase of the receiver may also be cycled, but this does not affect the density matrix ρ_n. Assuming the phase increments of the RF pulse and the receiver to be $\Delta\phi_k$ and $\Delta\phi_R$, respectively, consider a DM component that undergoes coherence order change Δp_k during the pulse k. Depending on the values of $\Delta\phi_k$ and $\Delta\phi_R$, the CTP in question may or may not be selected by the phase cycle. Phase cycling the RF pulse k modulates the phases of the operators in Eq. (33) as follows:

$$\begin{aligned}&H_k \rightarrow H_k e^{im\Delta\phi_k} \\ &\rho_k \rightarrow \rho_k e^{-im\Delta p_k \Delta\phi_k} \\ &[\rho_k, H_k] \rightarrow [\rho_k, H_k] e^{-im(\Delta p_k - 1)\Delta\phi_k}\end{aligned} \tag{34}$$

where m is the step of the phase cycle. The cycling of the receiver increments the phase of the observable operator:

$$I_-^+ \rightarrow I_-^+ e^{-im\Delta\phi_R} \tag{35}$$

Therefore, the error of the detected signal is cycled as:

$$Tr(I_-^+ \cdot U^+ [\rho_k, H_k] U) \rightarrow Tr(I_-^+ \cdot U^+ [\rho_k, H_k]_{step1} U)\, e^{-im(\Delta\phi_R + (\Delta p_k - 1)\Delta\phi_k)} \tag{36}$$

where $U = U_{k+1} \ldots U_n$. Although the operator U is not phase cycled, it needs to be kept on the RHS of Eq. (36) because it can affect whether the phase-cycled commutator contains detectable coherences. Equation (36) yields the condition for the survival of error in the phase cycle:

$$\Delta\phi_R = \Delta\phi_k \cdot (1 - \Delta p_k) + 2\pi j \tag{37}$$

The signal error from any CTPs that fail to satisfy Eq. (37) is cancelled out by the phase cycle. Equation (37) implies that any CTP selected by the phase cycle must have a zero contribution to the error of the phase-cycled signal: If the coherence order change Δp_k is selected by the pulse sequence, then

$$\Delta\phi_{\mathrm{R}} = -\Delta p_k \, \Delta\phi_k \tag{38}$$

and Eq. (36) takes the form

$$Tr(I_-^+ \cdot U^+[\rho_k, H_k]_{step1} U)\, e^{-im[-\Delta\rho_k\Delta\phi_k + \Delta\rho_k\Delta\phi_k - \Delta\phi_k]} = Tr(I_-^+ \cdot U^+[\rho_k, H_k]_{step1} U)\, e^{im\Delta\phi_k} \tag{39}$$

It can immediately be seen that a full phase cycle zeroes out the signal error from any CTP that is selected. In general, for an M-step phase cycle on pulse k incrementing the phase of H_k by $\Delta\phi_k$ and the phase of the receiver by $\Delta\phi_{\mathrm{R}}$, the contribution to the error of the phase-cycled signal is

$$\left(\frac{d\,S}{d\,\theta_k}\right)_{cycled} = \left(\frac{\partial\, S}{\partial\,\theta_k}\right)_{step\ 1} \cdot \frac{e^{-iM[\Delta\phi_{\mathrm{R}} + (\Delta p_k - 1)\Delta\phi_k]} - 1}{e^{-i[\Delta\phi_{\mathrm{R}} + (\Delta p_k - 1)\Delta\phi_k]} - 1} \tag{40}$$

A similar approach can be employed for the analysis of the phase-cycling behaviour of the errors arising from a mis-set phase of RF pulses. The appropriate error interrogation operator for a misset RF phase is shown in Eq. (15). Following the derivation similar to Eqs. (33) – (36), it is easy to see that the phase-cycling behaviour of RF phase errors can be presented as

$$Tr(I_-^+ \cdot U^+[\rho_k, R_k]U) = -i\,A\sin\theta_k \cdot e^{-im[\Delta\phi_{\mathrm{R}} + (\Delta p_k - 1)\Delta\phi_k]} + 2B\sin^2\frac{\theta_k}{2} \cdot e^{-im(\Delta\phi_{\mathrm{R}} + \Delta p_k\Delta\phi_k)} \tag{41}$$

where $A = Tr(I_-^+ \cdot [\rho_k, [I_z, H_{k\phi}]]_{step\ 1})$ and $B = Tr(I_-^+ \cdot [\rho_k, I_z]_{step\ 1})$. The first term in Eq. (41) is zero when the RF pulse in question is a RF π pulse; the survival of the RF phase error in this case is determined by the phase-cycling behaviour of the second term only. The second term in Eq. (41) is generally non-zero for both $\pi/2$ and π RF pulses. The survival rules are therefore different for these two situations. An example is considered in the Results and Discussion section ("Spin-echo pulse sequence: phase errors of the π pulse under phase cycling").

Appendix B: Phase cycling on an RF pulse other than the pulse mis-set

Phase cycling can also involve an RF pulse (θ_m) different from the interval varied (θ_k). Here we analyse $\partial S/\partial\theta_k$ for the case when the pulse cycled (m) occurs after the "mis-set" interval (k). The situation where m precedes k can be handled in a similar manner. In order to gain insight into the behaviour of the phase-cycled $\partial S/\partial\theta_k$, we employ a reverse unitary transformation where the detected signal is transformed to the time point k. Consider the derivative of the signal in the first step of the phase cycle:

$$\frac{\partial S}{\partial \theta_k} = i\,Tr\left(I_-^+ \cdot [\rho_n, U_n^+ \ldots U_{k+1}^+ \cdot H_k \cdot U_{k+1} \ldots U_n]\right) \tag{42}$$

Because the trace of an operator is invariant to a unitary transformation, the expression within the Tr() in Eq. (42) can be restated as:

$$\begin{aligned}\frac{\partial S}{\partial \theta_k} &= i\,Tr\left\{U_{k+1}\ldots U_n \cdot I_-^+ \cdot [\rho_n, U_n^+ \ldots U_{k+1}^+ \cdot H_k \cdot U_{k+1}\ldots U_n] \cdot U_n^+ \ldots U_{k+1}^+\right\} \\ &= i \cdot Tr\left\{I_-^{*+}(n:k+1) \cdot [\rho_k, H_k]\right\}\end{aligned} \tag{43}$$

where the following reverse-transformed observable operator is used:

$$I_-^{*+}(n:k+1) = U_{k+1}\ldots U_n \cdot I_-^+ \cdot U_n^+ \ldots U_{k+1}^+ \tag{44}$$

The effect of phase cycling the RF pulse $m > k$ on the derivative in Eq. (43) is solely to modify the operator $I_-^{*+}(n : k+1)$. The commutator $[\rho_k, H_k]$ is unchanged because none of the operators preceding the time point k are phase cycled. Therefore, the calculation of the phase-cycled $\partial S/\partial\theta_k$ is reduced to the calculation of the average value of the operator $I_-^{*+}(n : k+1)$ over the phase cycle. For phase cycling performed on the pulse m, this is given by

$$I_-^{*+}(n:k+1)_{PC} = \sum_q u_{k+1}\ldots u_{mq}\ldots u_n \cdot I_-^+ e^{-iq\Delta\phi_R} \cdot u_n^+ \ldots u_{mq}^+ \ldots u_{k+1}^+ \tag{45}$$

We call the operator given by Eq. (45) the phase-cycled reverse-transformed observable operator. The error of the phase-cycled signal is:

$$\left(\frac{d\,S}{d\,\theta_k}\right)_{PC} = i \cdot Tr\left\{ I_{-}^{*+}(n:k+1)_{PC} \cdot [\rho_k, H_k] \right\} \tag{46}$$

Appendix C: Second-order derivative of the final DM.

The formalism of Eq. (4) can be used to obtain an analytic expression for the second derivative of the final DM. Differentiating Eq. (4) one more time, we obtain

$$\begin{aligned}\frac{d^2\rho_n}{d\,\theta_k^2} &= U_n^+ \ldots U_{k+1}^+ \cdot (-H_k^2) \cdot U_k^+ \ldots U_1^+ \cdot \rho_0 \cdot U_1 \ldots U_n + \\ &+ U_n^+ \ldots U_{k+1}^+ \cdot (-iH_k) \cdot U_k^+ \ldots U_1^+ \cdot \rho_0 \cdot U_1 \ldots U_k \cdot (iH_k) \cdot U_{k+1} \ldots U_n + \\ &+ U_n^+ \ldots U_{k+1}^+ \cdot (-iH_k) \cdot U_k^+ \ldots U_1^+ \cdot \rho_0 \cdot U_1 \ldots U_k \cdot (iH_k) \cdot U_{k+1} \ldots U_n + \\ &+ U_n^+ \ldots U_1^+ \cdot \rho_0 \cdot U_1 \ldots U_k \cdot (-H_k^2) \cdot U_{k+1} \ldots U_n\end{aligned} \tag{47}$$

Terms 2 and 3 in Eq. (47) are identical but will be kept separate for the purposes of the derivation. Manipulation of the four terms yields:

$$\begin{aligned}&\text{Term 1}: \left(U_n^+ \ldots U_{k+1}^+ \cdot (-iH_k) \cdot U_{k+1} \ldots U_n\right) \cdot U_n^+ \ldots U_{k+1}^+ \cdot (-iH_k) \cdot U_k^+ \ldots U_1^+ \cdot \rho_0 \cdot U_1 \ldots U_n \\ &\text{Term 2}: \left(U_n^+ \ldots U_{k+1}^+ \cdot (-iH_k) \cdot U_{k+1} \ldots U_n\right) \cdot U_n^+ \ldots U_1^+ \cdot \rho_0 \cdot U_1 \ldots U_k \cdot (iH_k) \cdot U_{k+1} \ldots U_n \\ &\text{Term 3}: U_n^+ \ldots U_{k+1}^+ \cdot (-iH_k) \cdot U_k^+ \ldots U_1^+ \cdot \rho_0 \cdot U_1 \ldots U_n \cdot \left(U_n^+ \ldots U_{k+1}^+ \cdot (iH_k) \cdot U_{k+1} \ldots U_n\right) \\ &\text{Term 4}: U_n^+ \ldots U_1^+ \cdot \rho_0 \cdot U_1 \ldots U_k \cdot (iH_k) \cdot U_{k+1} \ldots U_n \cdot \left(U_n^+ \ldots U_{k+1}^+ \cdot (iH_k) \cdot U_{k+1} \ldots U_n\right)\end{aligned} \tag{48}$$

Addition of Terms 1 and 2 yields

$$\mathrm{T1} + \mathrm{T2} = -i \cdot H_k^*(k+1:n) \cdot i[\rho_n, H_k^*(k+1:n)] \tag{49}$$

Similarly, addition of Terms 3 and 4 gives

$$\mathrm{T3} + \mathrm{T4} = i[\rho_n, H_k^*(k+1:n)] \cdot iH_k^*(k+1:n) \tag{50}$$

The analytic expression for the second DM derivative is obtained by combining Eqs. (49) and (50); this is shown in Eq. (18) in the main text.

Table 1. Hamiltonians effective during different intervals of the CP and CPMG pulse sequences and the ideal density matrix at the *n*-th echo.

	CP	CPMG
Hamiltonian during π pulses	I_x	I_y
Hamiltonian during τ intervals	I_z	I_z
DM at the *n*-th echo	$(-1)^n I_y$	I_y

Table 2. Analytic cumulative first- and second-order derivatives of the DM at the *n*-th CP and CPMG echo with respect to the duration of the refocusing RF pulse, θ (nominal $\theta = \pi$).

		$\partial\rho_n/\partial\theta$	$\partial^2\rho_n/\partial\theta^2$
CP		$-(-1)^n n \cdot I_z \cos(\omega\tau)$	$-(-1)^n n \cdot I_x \frac{\sin(2\omega\tau)}{2} - (-1)^n n^2 \cdot I_y \frac{\cos(2\omega\tau)+1}{2}$
CPMG	Odd *n*	$-I_z \sin(\omega\tau)$	$-(-1)^n n \cdot I_x \frac{\sin(2\omega\tau)}{2} - I_y \frac{1-\cos(2\omega\tau)}{2}$
	Even *n*	0	$-(-1)^n n \cdot I_x \frac{\sin(2\omega\tau)}{2}$

Table 3. The effect of EXORCYCLE phase cycling on the density matrix errors arising from an off-resonance π pulse in the spin-echo experiment. ρ_4 is the density matrix at the top of the echo; $\Delta\omega$ is the resonance offset. The errors shown include the effects of both the off-resonance refocusing pulse and off-resonance evolution during the echo time. The phase-cycled quantities are: (Step 1) + (Step 3) after the 2-step cycle and (Step 1) – (Step 2) + (Step 3) – (Step 4) after the 4-step cycle (corresponding to the receiver cycled as $+x$, $-x$, $+x$, $-x$). The first derivative is zeroed out under the two-step phase cycle, but the second derivative survives the four-step phase cycle. The derivatives are shown down to the constant multiplier.

Phase of the π pulse	Step 1	Step 2	Step 3	Step 4	After 2-step phase cycle	After 4-step phase cycle
	x	y	$-x$	$-y$		
ρ_4	$+I_y$	$-I_y$	$+I_y$	$-I_y$	$+2I_y$	$+4I_y$
$\partial\rho_4/\partial\Delta\omega$	0	$-I_z$	0	I_z	0	0
$\partial^2\rho_4/\partial\Delta\omega^2$	$-I_y$	$+I_y$	$-I_y$	$+I_y$	$-2I_y$	$-4I_y$

Table 4. The effect of EXORCYCLE on the signal errors (ΔS) arising from a phase error of the refocusing π pulse in the spin-echo experiment. ρ_3 is the density matrix immediately after the π pulse. The signal error ΔS is identical in each step of the four-step phase cycle, corresponding to a constant phasing error of the acquired signal.

Phase cycle step	Step 1	Step 2	Step 3	Step 4
H_3	$+I_x$	$+I_y$	$-I_x$	$-I_y$
R_3	$2I_z$	$2I_z$	$2I_z$	$2I_z$
ρ_3	$I_x\sin\theta_2 - I_y\cos\theta_2$	$-I_x\sin\theta_2 + I_y\cos\theta_2$	$I_x\sin\theta_2 - I_y\cos\theta_2$	$-I_x\sin\theta_2 + I_y\cos\theta_2$
$[\rho_3, R_3]$	$-i(I_x\sin\theta_2 + I_y\cos\theta_2)$	$i(I_x\sin\theta_2 + I_y\cos\theta_2)$	$-i(I_x\sin\theta_2 + I_y\cos\theta_2)$	$i(I_x\sin\theta_2 + I_y\cos\theta_2)$
I_-^+	I_+	$-I_+$	I_+	$-I_+$
ΔS	$+\Delta$	$+\Delta$	$+\Delta$	$+\Delta$

Table 5. Analysis of the contributions from individual CTPs to the signal error in the magnitude COSY experiment. The derivative values ($\partial S/\partial\theta_3$) were obtained using the ECF [Eq. (7)] and verified using explicit density-matrix simulations as explained in text. The signal values (S) were obtained using explicit DM simulations. For the CTPs not shown here, both the signal and $\partial S/\partial\theta_3$ were identically equal to zero in each step of the phase cycle. The following parameters were used: ν_1 = 101.37 Hz, ν_2 = 250.59 Hz, J = 7.3 Hz, t_2 = 23.7 ms, t_4 = 57.31 ms. With these simulation parameters, the values of S and $\partial S/\partial\theta_3$ were as follows: a = 74.0733 − 2.85898 i; b = −32.3254 + 54.4154 i; c = 5.35607 − 0.206726 i; d = −68.7172 + 2.65225 i; e = −2.73754 + 4.60826 i; f = −35.0629 + 59.0236 i. S_0 was taken as 1000 arbitrary units. In each step of the phase cycle $p(H_3) = \pm 1$.

p_2	p_3	Step 1		Step 2		After phase cycle	
		S	$\partial S/\partial\theta_3$	S	$\partial S/\partial\theta_3$	S	$\partial S/\partial\theta_3$
–1	–2	0	c	0	c	0	2c
–1	–1	a	0	a	0	2a	0
–1	0	0	d	0	d		2d
1	–2	0	e	0	e	0	2e
1	–1	b	0	b	0	2b	0
1	0	0	f	0	f	0	2f

Table 6. The phase cycle of the DQF COSY pulse sequence shown in Fig. 6. In text we consider the effect on the signal of varying the duration of the second RF pulse (which is not phase-cycled): $\partial S/\partial\theta_3$.

P1	P2	P3	AQ
y	*x*	*y*	*x*
y	*x*	$-x$	$-y$
y	*x*	$-y$	$-x$
y	*x*	*x*	*y*

Table 7. Analysis of the contributions from individual CTPs to the signal error in the DQF COSY experiment. The signal and signal errors were simulated as in Table 5 with the following parameters: ν_1 = 101.37 Hz, ν_2 = 250.59 Hz, J = 7.3 Hz, t_2 = 23.7 ms, t_5 = 57.31 ms. The results were verified using explicit density-matrix simulations as explained in text. For the CTPs not shown, both the signal and the signal error were identically equal to zero in each step of the phase cycle. With the simulation parameters shown above the signal and error values were as follows: a = 2.67803 – 0.103363 i, b = 1.22276 + 31.6806 i, c = –31.6806 + 1.22276 i, d = 68.7172 – 2.65225 i, e = 1.36877 – 2.30413 i, f = 31.8159 + 18.9002 i, g = –18.9002 + 31.8159 i, h = –35.0629 + 59.0236 i, aa = –1.3390 + 0.0516816 i, bb = –0.103363 – 2.67803 i, cc = 4.01705 – 0.155045 i, dd = –2.67803 + 0.103363 i, ee = 31.6806 – 1.22276 i, ff = –34.3586 + 1.32613 i, gg = –2.65225 – 68.7172 i, hh = –0.684384 + 1.15207 i, ii = –2.30413 – 1.36877 i, jj = 2.05315 – 3.45620 i, kk = 1.36877 – 2.30413 i, ll = 18.9002 – 31.8159 i, mm = –17.5315 + 29.5118 i, nn = 59.02363 + 35.0629 i. S_0 = 1000 (arbitrary units); p_j is the coherence order at the end of interval j.

p_2	p_3	p_4	Step 1: $p[H_3*(4:5)] = 0$		Step 2: $p[H_3*(4:5)] = \pm 1$		Step 3: $p[H_3*(4:5)] = 0$		Step 4: $p[H_3*(4:5)] = \pm 1$		Phase-cycled	
			S	$\partial S/\partial\theta_3$	S	$\partial S/\partial\theta_3$	S	$\partial S/\partial\theta_3$	S	$\partial S/\partial\theta_3$	S	$\partial S/\partial\theta_3$
–1	–2	–2	0	0	0	*aa*	0	0	0	*–aa*	0	0
–1	–2	–1	*a*	*bb*	*a*	0	*a*	*–bb*	*a*	0	4*a*	0
–1	–2	0	0	0	0	*cc*	0	0	0	*–cc*	0	0
–1	–1	–2	0	0	0	*dd*	0	0	0	*dd*	0	2*dd*
–1	–1	–1	*b*	*ee*	*c*	0	*–b*	*ee*	*–c*	0	0	2*ee*
–1	–1	0	0	0	0	*ff*	0	0	0	*ff*	0	2*ff*
–1	0	–1	*d*	*gg*	*–d*	0	*d*	*–gg*	*–d*	0	0	0
–1	1	–2	0	0	0	*–dd*	0	0	0	*–dd*	0	*–2dd*
–1	1	–1	*–b*	*–ee*	*c*	0	*b*	*–ee*	*–c*	0	0	*–2ee*
–1	1	0	0	0	0	*–ff*	0	0	0	*–ff*	0	*–2ff*
–1	2	–2	0	0	0	*–aa*	0	0	0	*aa*	0	0
–1	2	–1	*a*	*bb*	*a*	0	*a*	*–bb*	*a*	0	4*a*	0
–1	2	0	0	0	0	*–cc*	0	0	0	*cc*	0	0
1	–2	–2	0	0	0	*hh*	0	0	0	*–hh*	0	0
1	–2	–1	*e*	*ii*	*e*	0	*e*	*–ii*	*e*	0	4*e*	0
1	–2	0	0	0	0	*jj*	0	0	0	*–jj*	0	0
1	–1	–2	0	0	0	*kk*	0	0	0	*kk*	0	2*kk*
1	–1	–1	*f*	*ll*	*g*	0	*–f*	*ll*	*–g*	0	0	2*ll*
1	–1	0	0	0	0	*mm*	0	0	0	*mm*	0	2*mm*
1	0	–1	*h*	*nn*	*–h*	0	*h*	*–nn*	*–h*	0	0	0
1	1	–2	0	0	0	*–kk*	0	0	0	*–kk*	0	*–2kk*
1	1	–1	*–f*	*–ll*	*g*	0	*f*	*–ll*	*–g*	0	0	*–2ll*
1	1	0	0	0	0	*–mm*	0	0	0	*–mm*	0	*–2mm*
1	2	–2	0	0	0	*–hh*	0	0	0	*hh*	0	0
1	2	–1	*e*	*ii*	*e*	0	*e*	*–ii*	*e*	0	4*e*	0
1	2	0	0	0	0	*–jj*	0	0	0	*jj*	0	0

Table 8. The phase cycle of the Jeener-Broekaert pulse sequence shown in Fig. 7.

P1	P2	P3	P4	AQ
x	*x*	*y*	*x*	*x*
x	*x*	*y*	*y*	*y*
x	*x*	*y*	$-x$	$-x$
x	*x*	*y*	$-y$	$-y$

Figure Captions

Fig. 1 A general representation of an NMR pulse sequence and the notation used in the present work. The intervals t_1, t_2,... can represent RF pulses, gradient pulses and evolution delays. The generalised times θ_k and the spin Hamiltonians H_k are both dimensionless, as explained in text. The rotating-frame spin Hamiltonian within each interval is assumed to be constant.

Fig. 2 The Carr-Purcell (CP) and Carr-Purcell-Meiboom-Gill (CPMG) experiments. The two experiments differ by the phase of the refocusing π pulses: $\alpha = x$ for CP and $\alpha = y$ for CPMG. Vertical arrows indicate the echoes. In Results and Discussion, the effects of mis-setting the duration of the refocusing pulses are considered.

Fig. 3 The I_x, I_y and I_z components of the DM errors of CP and CPMG echoes as a function of n. The errors plotted are the Taylor expansions around $\theta = \pi$ truncated at the sixth-order derivative. The derivatives were obtained using the error commutator formalism. Parameters used: $\omega\tau = 2$, miscalibration of the refocusing π pulse $\delta\theta = -\pi/18$, spin relaxation was neglected. The errors are shown as a fraction of the equilibrium magnetisation, M_0. In both plots, the dashed, the solid and the dotted lines represent the relative errors of I_x, I_y and I_z, respectively. The ECF errors were compared to the "exact" errors computed by explicitly simulating the evolution of the DM under mis-set refocusing pulses (not shown) and matched the latter to within 0.001% of M_0 for both CP and CPMG.

Fig. 4 Spin Echo pulse sequence: $\theta_1 = \pi/2$, $\theta_3 = \pi$ and $t_2 = t_4$. The phase cycle used is the four-step EXORCYCLE [12]: the $\pi/2$ RF pulse has a constant phase $+x$; the phase of the π pulse is cycled as $+x$, $+y$, $-x$, $-y$; and the receiver is cycled as $+x$, $-x$, $+x$, $-x$.

Fig. 5 (A) The magnitude COSY pulse sequence. (B) Coherence transfer pathways for a system of two scalar-coupled spins-1/2. The solid lines show the observable CTPs. The dashed lines show the CTPs contributing to the error of the phase-cycled signal. As explained in text, only the CTPs that: (1) end in $p_4 = 0$ or -2 and (2) exhibit $\Delta p_3 = 1, -1$ or -3 contribute to the error of the phase-cycled signal.

Fig. 6 Double-quantum filtered COSY pulse sequence [43,44]. The phase cycle selecting double quantum-filtered CTPs is shown in Table 6.

Fig. 7 Jeener-Broekaert pulse sequence used to select the NMR signal from quadrupolar nuclei in partially aligned environments [9,37]. The second $\pi/4$ RF pulse and the receiver are phase-cycled according to Table 8. The perfect selection of quadrupolar order requires that the phases of the $\pi/2$ pulse and the first $\pi/4$ RF pulse be orthogonal. The time between the two $\pi/4$ pulses is assumed to be negligibly small.

Fig. 8 Jeener-Broekaert spectra of a mixture of single spin-1 nuclei in a partially aligned environment (60%; $\omega_0 = 1113$ Hz; $\omega_Q = 2000$ Hz) and an isotropic environment (40%; $\omega_0 = 1113$ Hz): (a) numerical density-matrix simulation assuming the perfectly orthogonal phases P1 and P3 (see Table 8); (b) numerical density-matrix simulation with the phase of the first $\pi/4$ pulse slightly mis-set (P3 = 0.48π); (c) the difference between (b) and (a); (d) the difference between the two spectra obtained using the ECF [Eq. (14)]. The ECF difference spectrum matches that computed in explicit DM simulations.

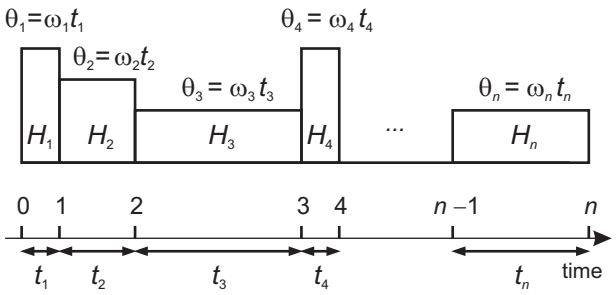

Figure 1, Momot and Takegoshi, Robustness of NMR pulse sequences

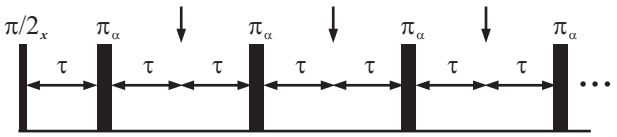

Figure 2, Momot and Takegoshi, Robustness of NMR pulse sequences

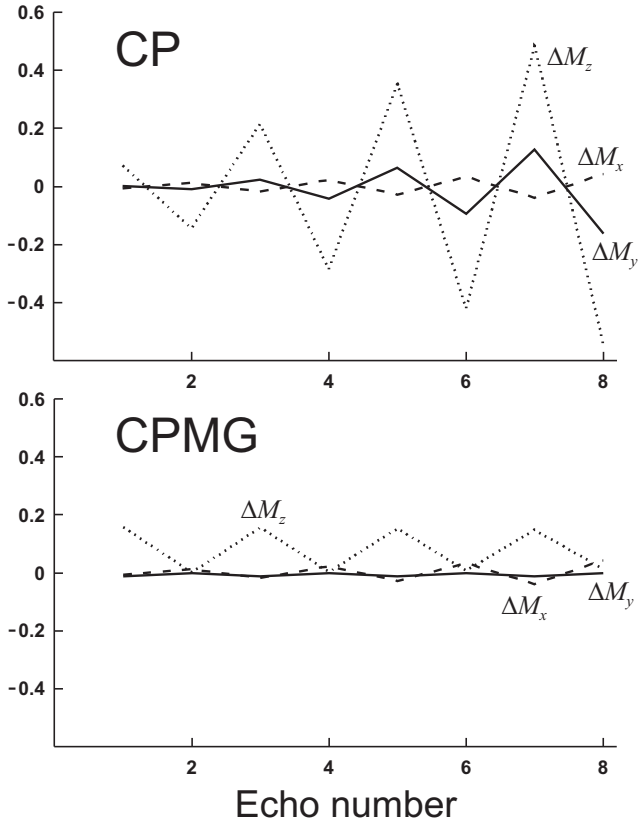

Figure 3, Momot and Takegoshi, Robustness of NMR pulse sequences

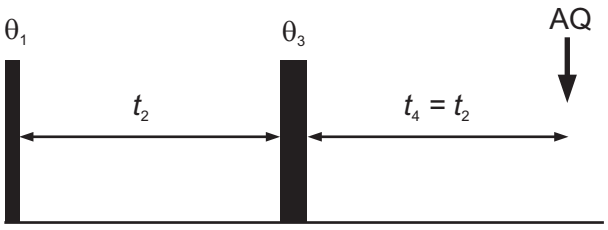

Figure 4, Momot and Takegoshi, Robustness of NMR pulse sequences

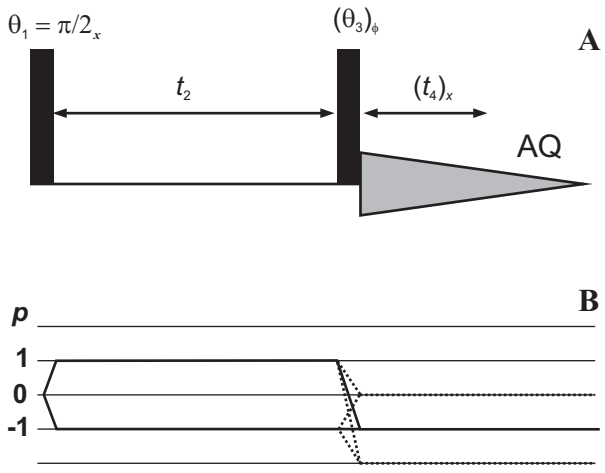

Figure 5, Momot and Takegoshi, Robustness of NMR pulse sequences

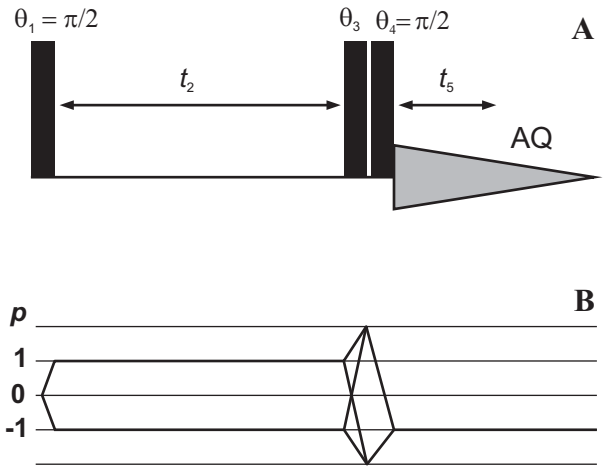

Figure 6, Momot and Takegoshi, Robustness of NMR pulse sequences

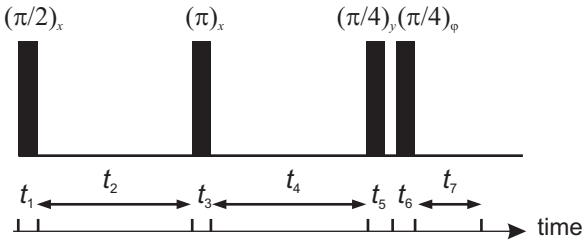

Figure 7, Momot and Takegoshi, Robustness of NMR pulse sequences

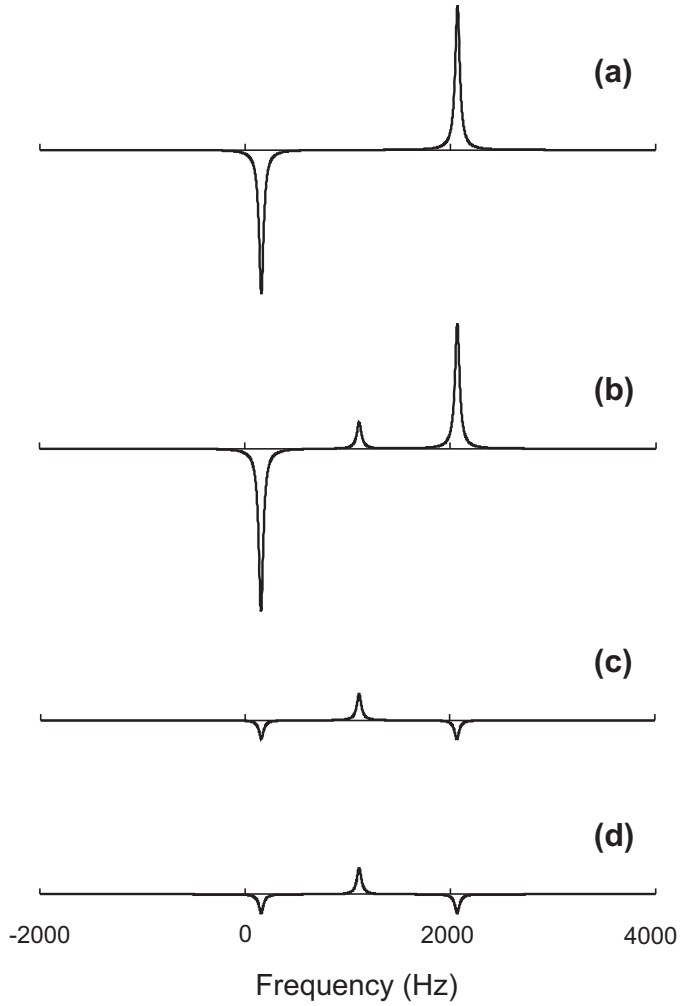

Figure 8, Momot and Takegoshi, Robustness of NMR pulse sequences